scientific reports

Check for updates

OPEN

Behavioral, neural and ultrastructural alterations in a graded-dose 6-OHDA mouse model of early-stage Parkinson's disease

Andrea Slézia[1,2,3,4,7]✉, Panna Hegedüs[1,5,7], Evgeniia Rusina[2,7], Katalin Lengyel[1], Nicola Solari[1], Attila Kaszas[4], Diána Balázsfi[1], Boris Botzanowski[2], Emma Acerbo[2], Florian Missey[2], Adam Williamson[2,6]✉ & Balázs Hangya[1]✉

Studying animal models furthers our understanding of Parkinson's disease (PD) pathophysiology by providing tools to investigate detailed molecular, cellular and circuit functions. Different versions of the neurotoxin-based 6-hydroxydopamine (6-OHDA) model of PD have been widely used in rats. However, these models typically assess the result of extensive and definitive dopaminergic lesions that reflect a late stage of PD, leading to a paucity of studies and a consequential gap of knowledge regarding initial stages, in which early interventions would be possible. Additionally, the better availability of genetic tools increasingly shifts the focus of research from rats to mice, but few mouse PD models are available yet. To address these, we characterize here the behavioral, neuronal and ultrastructural features of a graded-dose unilateral, single-injection, striatal 6-OHDA model in mice, focusing on early-stage changes within the first two weeks of lesion induction. We observed early onset, dose-dependent impairments of overall locomotion without substantial deterioration of motor coordination. In accordance, histological evaluation demonstrated a partial, dose-dependent loss of dopaminergic neurons of substantia nigra pars compacta (SNc). Furthermore, electron microscopic analysis revealed degenerative ultrastructural changes in SNc dopaminergic neurons. Our results show that mild ultrastructural and cellular degradation of dopaminergic neurons of the SNc can lead to certain motor deficits shortly after unilateral striatal lesions, suggesting that a unilateral dose-dependent intrastriatal 6-OHDA lesion protocol can serve as a successful model of the early stages of Parkinson's disease in mice.

Abbreviations

PD	Parkinson's disease
6-OHDA	6-Hydroxy-dopamine
DA	Dopamine
DAergic	Dopaminergic
SNc	Substantia nigra pars compacta
TH	Tyrosine-hydroxylase
TH +	Tyrosine-hydroxylase immunopositive
LD	Low dose

[1]Institute of Experimental Medicine, Lendület Laboratory of Systems Neuroscience, Budapest, Hungary. [2]Institut de Neurosciences Des Systèmes, INSERM UMR S 1106, Aix-Marseille Université, Marseille, France. [3]Institute of Cognitive Neuroscience and Psychology, Eotvos Lorand Research Network, Budapest, Hungary. [4]Institut de Neurosciences de la Timone, CNRS UMR 7289, Aix-Marseille Université, Marseille, France. [5]János Szentágothai Doctoral School of Neurosciences, Semmelweis University, Budapest, Hungary. [6]International Clinical Research Center (ICRC), St. Anne's University Hospital, Brno, Czech Republic. [7]These authors contributed equally: Andrea Slézia, Panna Hegedüs and Evgeniia Rusina. ✉email: andrea.slezia@gmail.com; adam.williamson@fnusa.cz; hangya.balazs@koki.hu

MD	Medium dose
HD	High dose

Parkinson's disease (PD) is the second most common neurodegenerative disorder affecting more than seven million people worldwide[1–4]. PD is a progressive neurodegenerative disease dominated by motor deficits including resting tremor, bradykinesia, rigidity, and postural instability, caused by the selective, large scale, irreversible degeneration of dopaminergic (DAergic) neurons mostly located in the substantia nigra pars compacta (SNc) of the midbrain. Non-motor symptoms, some of which often precede the onset of motor deficits, are also common among PD patients. These include hyposmia, autonomic dysfunction, sleep disturbances, depression, and cognitive impairment[5]. The gradually progressing, selective SNc DAergic cell loss leads to a progressive reduction of dopamine (DA) concentration in the striatum[6,7]. To date, there are no disease-modifying therapies that slow, halt, or reverse the progression of PD[8].

Importantly, the above-mentioned symptoms become apparent, and thus the diagnosis is usually made, at a rather advanced stage of neurodegeneration; on average, 50–80% of nigral DA neurons are already lost by that time[6,9,10]. Even though there are more and more studies on the early stages[11–18], this aspect of the disease still needs to be explored in greater detail. Neurodegenerative processes start to play a role in the manifestation of the disease decades before the diagnosis[3,19], including disrupted synaptic and cellular plasticity and consequential impairments of functional connectivity that eventually lead to motor and non-motor symptoms associated with PD[20,21]. Detailed behavioral analysis can help to better understand these network changes and aid PD diagnosis at an earlier timepoint, possibly allowing a timely clinical intervention[13,22,23]. Therefore, it is important to develop and improve research models that can help us pinpoint mechanisms of early changes in brain function during disease. In particular, graded models will allow a more differentiated picture of disease symptoms by enabling us to study both mild and severe lesions and correlated pathophysiological features at different stages of progression[24,25], potentially opening the way to novel neuroprotective therapies and early intervention or prevention of PD[26].

Here, we studied the histological and behavioral alterations that characterize the early stages of PD in a graded 6-OHDA mouse model. Our results from open field and rotarod behavioral assays show that mild motor impairments are detectable already at very early stages, even one week after a single low dose of striatal 6-OHDA injection, typically not explored in 6-OHDA models of PD. However, motor impairments mostly manifested in altered general horizontal locomotion and initiation of explorative locomotion, rather than in motor coordination, which was regularly found affected by PD at later stages[27,28]. While the mild impairment in exploratory motor behavior was maintained and aggravated after the second week in a dose-dependent manner, motor coordination probed by the rotarod test remained similar across 6-OHDA-injected and sham-operated mice. Motor symptoms were accompanied by a significant dose-dependent loss of DAergic cells in the SNc already after one week post injection. Additionally, ultrastructural changes in SNc DAergic neurons, such as the degeneration of mitochondria (swelling, structural changes of the lamellae) and the endoplasmic reticulum were detected by electron microscopy.

While we focused on characterizing the early onset motor deficits above, it is not yet fully clear to what extent different rodent models, including the toxin approach used here, reproduce the diverse non-motor pathology of PD. Nevertheless, many of the non-motor symptoms have been described in 6-OHDA lesioned rats. Bilateral 6-OHDA lesions in rats lead to increased anxiety[29] and depression-like[30] behaviors. Unilateral 6-OHDA injections into the rat medial forebrain bundle (MFB) or SNc lead to bladder dysfunction[31,32]. Rats undergoing unilateral 6-OHDA lesions of the MFB also showed delayed gastric emptying, which may have a mechanism similar to the constipation observed as a typical early sign of PD[33]. While motor symptoms have been reported to complicate the assessment of some PD-related non-motor dysfunctions in animal models of PD, we only found limited motor disabilities in our model, which may therefore be especially helpful in scoring non-motor deficits and thus further aid early PD diagnostics. As a caveat, however, the non-specific nature of most of these symptoms hampered previous efforts to use non-motor features as biomarkers of PD and thus additional, more-specific behavioral, genetic and/or biochemical markers will have to be identified[16,18,5].

In sum, our findings demonstrate the presence of early-onset structural and behavioral impairments in a single-dose, unilateral striatal 6-OHDA mouse model of PD, suggesting that the partial lesion protocol we developed might be suitable for investigating motor and non-motor changes in early phases of the disease, holding the promise for developing early diagnostics and interventions saving many disability-adjusted life years.

Materials and methods

Animals

Fourty-seven adult male C57BL6/J (8–10 weeks-old at the time of the drug-injection) mice were used for the experiments. Fourty-one mice underwent injection surgery: n = 11 mice received low-dose (LD), n = 10 medium-dose (MD) and n = 10 high-dose (HD) of 6-OHDA; 10 sham-operated mice received control injections. During the first week 1 MD, 1 HD and 1 sham animal died, and 3 sham-injected animals could not be tested for behavior due to injuries on their toes, resulting in a test population of n = 11 LD, n = 9 MD, n = 9 HD and n = 6 sham mice for the first round of behavioral testing. Of these mice, n = 4 LD, n = 4 MD, n = 4 HD and n = 1 sham mice were sacrificed and processed for immunohistochemistry after the first round of tests, while the remaining mice (LD, n = 7; MD, n = 5; HD, n = 5; sham, n = 5) underwent an additional week of testing followed by immunohistochemistry procedures. An additional n = 6 mice were used for electron microscopy experiments. Mice were kept on a 12 h light/dark cycle with food and water available ad libitum. All experiments were approved by the Committee for Scientific Ethics of Animal Research of the National Food Chain Safety Office (PE/EA/784–7/2019) and were performed according to the guidelines of the institutional ethical code and the Hungarian Act of Animal Care

and Experimentation (1998; XXVIII, section 243/1998, renewed in 40/2013) in accordance with the European Directive 86/609/CEE and modified according to the Directive 2010/63/EU and the ARRIVE guidelines.

Surgical procedure

Animals were briefly sedated with isoflurane (Forane-abbvie Hungaropharma, Hungary) in a sealed container (15–30 s) to reduce the stress associated with anesthesia. Buprenorphine analgesic was administered subcutaneously (Bupaq, 10%, 0.05–0.2 mg/kg, Primavet, Austria). Surgery was performed under ketamine-xylazine anesthesia (i.p. ketamine: 50 mg/kg; xylazine: 20 mg/kg, Medicus Partner, Netherlands). The depth of the anesthesia was monitored by checking reflexes, breathing frequency, and whisker movements. When adequate anesthesia was reached, animals were placed into a stereotaxic apparatus (Stoelting, UK).

The skin over the calvaria was shaved and disinfected with Betadine (EGIS, Hungary). Eyes were protected from dehydration and strong light with rodent eye ointment (Bausch & Lomb, Germany), repeated during surgery as necessary. The skin and connective tissues over the skull were infused by local anesthetics (Ropivacaine s.c., Braun Melsungen AG., Germany), and a midline scalp incision was made. Subcutaneous tissues were removed, the skull was cleaned, and the dura mater was removed. The head of the animal was adjusted so that Bregma and Lambda were in the same horizontal plane. A craniotomy was made over the left dorsal striatum (stereotaxic coordinates from bregma: anteroposterior 0.6 mm and mediolateral 1.8 mm)[34–36]. A borosilicate capillary pipette (Sutter Instrument, Germany) was lowered to the target area (dorsoventral – 2.0 mm from the cortical surface) and 6-OHDA (Sigma-Aldrich, Hungary) was injected by a syringe pump (World Precision Instruments, UK), delivering 1 µl of 6-OHDA solution diluted in 0.02% ascorbic acid (Sigma-Aldrich, Hungary) with a speed of 1 µl/min in either a low, medium or high dose (2.5 µg/µl, 5 µg/µl or 8 µg/µl 6-OHDA, respectively; Fig. 1A,B)[24]. For sham surgeries, we used the same stereotaxic coordinates and injected 1 µl of 0.02% ascorbic acid. The pipette was removed after 3–4 min waiting time and the wound edges were stitched or closed by Vetbond surgical glue (3M, Hungary). The animals were continuously monitored and observed for signs of pain, distress, or neurological complications for a one-week recovery time following the surgery.

Standard surgical procedures were carefully used to minimize animal suffering, brain tissue damage, and risk of infection. Operated mice were kept in separate cages. They were checked regularly in a 48-h postoperative period. Changes in body weight were monitored for three days after the surgery. While no specific handling protocol was applied, experimenters regularly interacted with mice during weight measurements and cage maintenance, thus reducing stress introduced by handling by the time of behavioral measurements.

Evaluation of locomotor activity, exploration, motor coordination, and voluntary movement

Open field test—measurement of spontaneous locomotor activity, movement initiation, and exploration

Animals were brought to the test room 20–30 min before behavioral testing to allow a period of settling after transportation. We did not habituate mice to the behavioral apparatus to avoid rapid loss of interest in the open field test as well as developing alternative or compensatory strategies on the rotarod that can potentially mask the effects of the lesions. Mice were placed separately in a $40 \times 40 \times 30$ cm plastic box with a 4×4 square mesh on its bottom and were video-recorded for 5 min (Fig. 1C,D). The following parameters of locomotion were extracted: (1) distance in cm, (2) speed in cm/min, (3) number of immobility periods, and (4) number of asymmetric rotations. The movement trajectories of mice were detected in the videos and were further analyzed by Image J software and Animal Tracker plugin[37], where overall distance covered, speed, the number of line crossings and spontaneous rotations were measured. Immobility periods were defined as events when mice were in the same cm^2 for at least 2s.

Rotarod test—testing motor coordination

Motor coordination was tested with rotarod equipment (Bioseb, France; Fig. 1E). To evaluate motor coordination and balance, the animals were placed on an accelerating rotating cylinder and the latency until falling from the rotating rod was measured. We used an accelerating speed from 4 to 40 RPM. The tests lasted for a maximum of 3 min and were repeated three times for each mouse with a five-minute break after each session. We measured the latency to fall and the RPM rotation speed at the time of fall. While some studies observed that mice are able to grip the rotating rod and spin with it without falling, we did not observe this type of behavior. During breaks, mice were placed in their own cages. For the rotarod test we did not do any previous training to avoid potential confounding factors (e.g. lesioned mice may learn more slowly but eventually achieve a performance level comparable to that of the study group).

Statistical analysis of behavioral tests

Statistical analyses were performed using one-way standard analysis of variance by using the GraphPad Prism 6.01 software (GraphPad Inc., San Diego, CA, USA). When a significant difference was found between groups, we performed Tukey's honest significant difference (HSD) post hoc multiple comparison test to identify pairwise differences. For all tests, $p \leq 0.05$ was considered significant.

Evaluation of neurodegenerative processes

Immunohistochemistry—visualizing DAergic cell loss

Histological evaluations were made in all animals that participated in the behavioral tests. Mice were euthanized with an overdose of pentobarbital (100 mg/kg i.p.). Animals were transcardially perfused first with saline, then with 150 ml of a fixative solution containing 4% paraformaldehyde (PFA) in 0.1 M phosphate buffer (PB). Tissue blocks were cut on a Vibratome (Leica VT1200S, Leica Microsystems, Wetzlar, Germany) into 50 µm coronal sections.

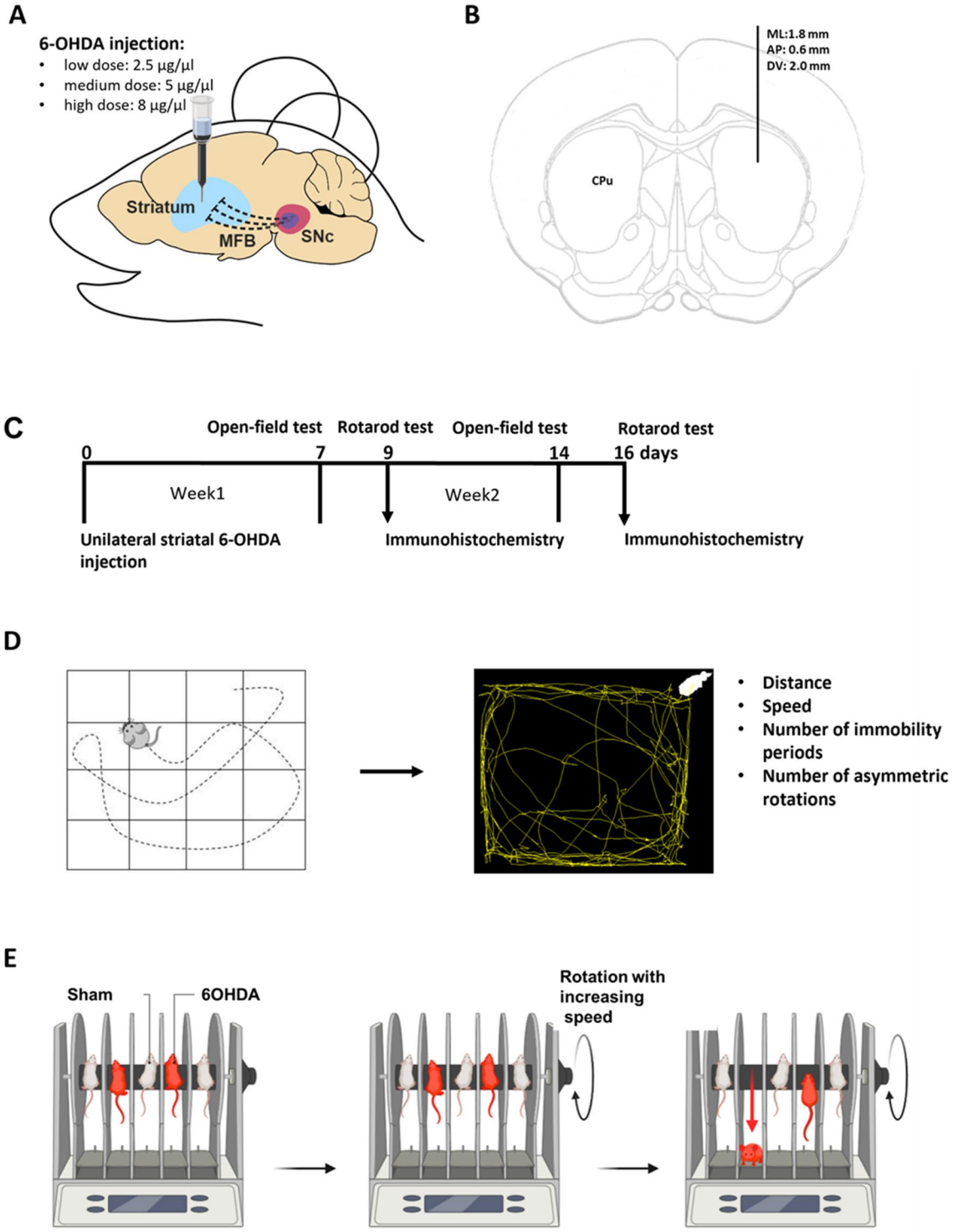

Figure 1. Methodological overview. (**A**) Schematic representation of the unilateral intrastriatal 6-OHDA injection. (**B**) Intrastriatal injection site marked in the mouse brain atlas in the coronal plane. Eleven low-dose (LD), 10 medium-dose (MD) and 10 high-dose (HD) mice and 10 sham-operated mice received injections. During the first week 1 MD, 1 HD and 1 sham animal died, and 3 sham-injected animals could not be tested for behavior due to injuries on their toes, resulting in a test population of n = 11 LD, n = 9 MD, n = 9 HD and n = 6 sham mice for the first round of behavioral testing. (**C**) Timeline of the experiment. Open field test was performed 7 and 14 days after 6-OHDA injection. Rotarod test was performed 9 and 16 days after the lesion. Of the mice tested in the first round, n = 4 LD, n = 4 MD, n = 4 HD and n = 1 sham mice were sacrificed and processed for immunohistochemistry after the first rotarod test, while the remaining mice (LD, n = 7; MD, n = 5; HD, n = 5; sham, n = 5) underwent an additional week of testing followed by immunohistochemistry procedures (see Materials and Methods). (**D**) Schematic representation of the open field test protocol and analysis. E, Schematic representation of the rotarod test protocol. The figure was created with BioRender.com.

After slicing and extensive washing in 0.1 M PB (3 times for 10 min), the 50-µm-thick sections were incubated in 30% sucrose overnight, freeze-thawed over liquid nitrogen four times, then processed for immunohistology. All following washing steps and dilutions of the antibodies were done in 0.05 M TBS buffer (pH = 7.4). After extensive washing in TBS (3 times for 10 min), the sections were blocked in 5% normal goat serum for 45 min and then incubated in the primary antibody for a minimum of 48 h at 4 °C (mouse anti-tyrosine hydroxylase monoclonal antibody recognizing an epitope in the mid-portion of the rat TH protein; dilution: 1:8000; Product No: 22941; ImmunoStar). After incubating with the primary antibody, the sections were treated with biotinylated donkey-anti-mouse IgG (1:300; Vector Laboratories) for 2 h. Next, the sections were incubated with avidin biotinylated–horseradish peroxidase complex (1:500; Elite ABC; Vector Laboratories) for 1.5 h. The immunoperoxidase reactions were finally developed using 3,3′-diaminobenzidine 4HCl (DAB) as the chromogen. Sections were dehydrated in xylol, then mounted in chrome-gelatin and covered by DePeX[38]. Correct localization of the injection sites was verified using sections of the striatum in all injected animals (Supplementary Fig. S1).

Neuronal counts—quantifying DAergic cell loss

Cell counting was performed in 4 animals from each group. Following the transcardial perfusion of the animals, blocks of both hemispheres (the injected ipsilateral and the contralateral side) were cut from the striatum up to the posterior-most part of the substantia nigra (from antero-posterior coordinates + 1.87 mm to–4.44 mm[34–36]. Next, 50 µm coronal sections were cut with a Vibratome (Leica VT1200S, Leica Microsystems, Wetzlar, Germany).

Serial sections were collected in 6 vials using the 'alternating sectioning' method[39–45]. During the cutting process, the first 50 µm coronal section was placed in the first vial, the second section in the second vial, up to the 6th vial. Then a new series was started, where the 7th section was placed in the first vial. The antero-posterior (AP) distance of 6 × 50 = 300 µm between the closest sections in each vial allowed for the clear identification of coronal sections, based on the difference in anatomical landmarks. Maintaining the serial order of the vials allowed us to identify neighboring sections (see also single cell axon and dendritic reconstructions in Refs.[39–42,46]).

Out of the six vials, three non-consecutive vials (#1, #3, #5 or #2, #4, #6) were selected for TH DAB immunostaining. All sections of the three non-consecutive vials were subjected to mouse anti-tyrosine hydroxylase (TH) monoclonal antibody immunoreaction using 3,3′-diaminobenzidine 4HCl (DAB) as the chromogen, mounted on microscopy slides and examined by brightfield microscopy. The AP level of each section was carefully defined based on the nuclei and the structures of the ipsi- and contralateral hemispheres, including the cortical layers, dorsal hippocampus, the ventrobasal system of the thalamus, zona incerta, subthalamic nucleus, lemniscus medialis etc. using mouse brain atlases. Sections containing the SNc were selected, then the AP level of each section was determined, then sections were further grouped to three subgroups (Fig. 5) on the basis of their AP levels. Thus, sections containing the SNc were used for quantitative analysis after careful assessment of the AP position of the sections[34–36].

TH immunostaining was carried out on 50 µm coronal sections containing SNc and ventral tegmental area (VTA) according to the immunoperoxidase protocol described above. The number of TH + cells per unit area was determined. For the estimation of dopaminergic cell loss, we used a method of Rice et al.[47,48]. The loss of DAergic neurons was determined by counting TH-immunoreactive cells under bright-field illumination. Each section was photographed using a 10× objective by randomly setting a fixed point in the Z axis within the section (Zeiss, LSM, Nikon Eclipse, Nikon 50i, 600 dpi uncompressed TIFF file). One to five nonoverlapping images were taken from each section to cover the entire SN/VTA complex within the section on both treated and non-treated sides. Each image was considered a "counting frame" with the bottom and right margins of the image as the forbidden lines of the counting frame. Neurons were selected for counting only if the entire cell body and the nucleus were clearly identified in the image. Neurons touching the right and bottom borders of the frame were excluded from counting. During the counting process, 8 to 12 sections were used in each animal, with 50 µm section intervals, while the shrinkage factor was defined from 3 to 5. The measured tissue thickness ranged between 10 and 15 µm [39,47]. The "cell counter" plug-in of NIH Image J software was used for the manual labeling of dopaminergic neurons in the images[48].

Statistical analysis of histological evaluation

Taking the cell numbers from the ipsilateral side of each slice as 100%, we calculated the cell number percentage on the contralateral, injected side, and these percentages were analyzed by one-way ANOVA using GraphPad Prism 6.1 software[47,48]. When a significant difference was found between groups, we performed Tukey's honest significant difference (HSD) post hoc multiple comparison test to identify pairwise differences. For all tests, $p \leq 0.05$ was considered significant.

Electron microscopy—visualizing ultrastructural changes in DAergic neurons

Regions of interest were selected for further analysis of labeled TH + neurons by immunohistochemistry and electron microscopy. For electron microscopic imaging, SNc and striatum were localized in 50 µm coronal sections using the mouse brain atlas as a reference. SNc and striatal tissue samples were dissected with a surgical scalpel from each section. Tissue samples were then mounted on epoxy blocks for ultramicrotome sectioning[34–36].

Fifty µm sections were cryo-protected in 30% sucrose in PB overnight. The next day, sections were freeze-thawed: immersed in 30% sucrose solution at 4 °C overnight, then frozen over liquid nitrogen, then thawed on room temperature three times. Subsequently, tissue slices were washed in 0.1 M PB buffer. For intracellular detection of TH, the sections were washed subsequently in 0.1 M PB for 30 min, followed by washing in tris-buffered saline (TBS) and a 15 min treatment with borohydride in TBS. After washing out the borohydride with TBS, the sections were blocked in 1% human serum albumin (HSA; Sigma-Aldrich) in TBS for 1 h. Then, they

were incubated in a solution of primary antibodies against TH (mouse, 1:8000 in TBS). Next, the sections were incubated in a secondary antibody solution containing gold-conjugated donkey anti-mouse (donkey-anti-mouse IgG (H&L) Ultra Small, Aurion; in a concentration of 1:100) diluted in Gel-BS. After intensive washes in BSA-c, the sections were treated with 2% glutaraldehyde in 0.1 M PB for 15 min to fix the gold particles into the tissue. To enlarge immunogold particles, this was followed by incubation in silver enhancement solution (SE-EM; Aurion) for 1h at room temperature. The sections were treated with 0.5% osmium tetroxide in 0.1 M PB on ice and they were dehydrated in ascending alcohol series and in acetonitrile and embedded in Durcupan (ACM; Fluka). During dehydration, the sections were treated with 1% uranyl acetate in 70% ethanol for 20 min. After this, 60-nm-thick serial sections were prepared using an ultramicrotome (Leica EM UC6) and picked up on single-slot copper grids. The sections were examined using a Hitachi H-7100 electron microscope and a Veleta CCD camera.

Results

Behavioral tests

Locomotion in open field test

Mice received unilateral injections of 6-OHDA in the dorsal striatum at three different doses (Supplementary Fig. S1). Overall horizontal locomotion was tested in an open field (OF) arena 1 week and 2 weeks after injections to assess early impairments potentially relevant to PD onset[28] (Fig. 2). We measured the average speed, and the number of times mice crossed the lines of a grid across the arena ('number of line-crossings') during the full 5 min duration of the OF test[27].

One week after injection, we observed an acute, dose-dependent disruption of overall motility. Importantly, low dose (LD) injections did not lead to significant or even tendentious changes in average speed and number of line-crossings tested one-week post-injection (average speed, $p = 0.6428$; number of line crossings, $p = 0.9823$; one-way ANOVA, Tukey's multiple comparison test; Fig. 2A,C). At the same time, the average speed was significantly lower, and the number of line-crossings also decreased significantly in mice receiving medium dose

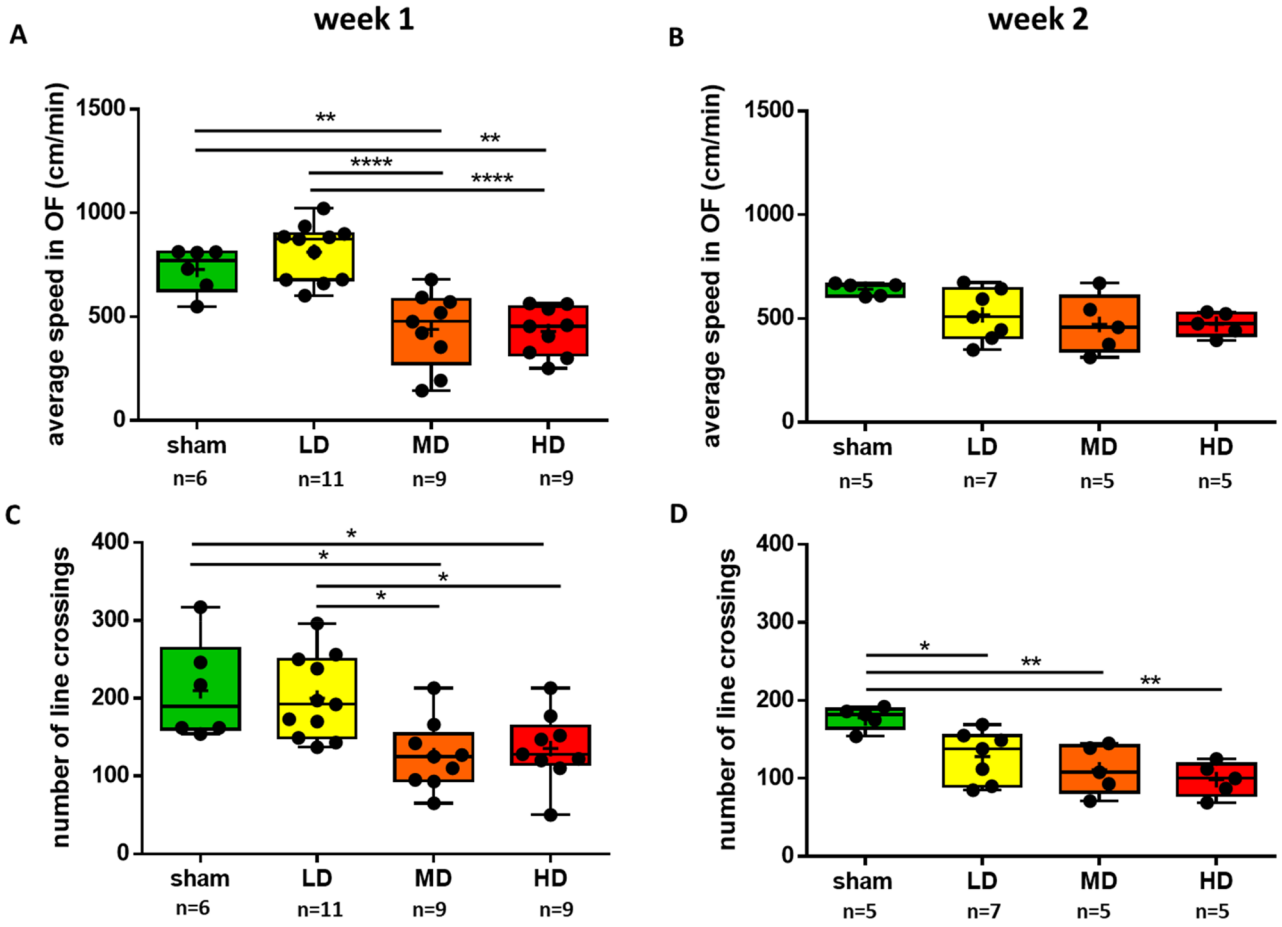

Figure 2. Overall horizontal locomotion showed early impairment after partial unilateral striatal 6-OHDA lesion. (**A**) Average speed in an open field arena was measured one week after the lesion protocol. (**B**) In half of the animals, the measurements were repeated two weeks after the lesion. (**C**) The 'number of line crossings' in the OF (see Fig. 1) was measured one week post lesion. (**D**) The 'number of line crossings' in the OF (see Fig. 1) was measured two weeks post lesion. LD, low dose; MD, medium dose; HD, high dose. *, $p \leq 0.05$; **, $p \leq 0.01$; ***, $p \leq 0.001$; ****, $p \leq 0.0001$.

(MD) and high dose (HD) injections compared to sham-lesioned mice (average speed: sham vs. MD, $p = 0.0026$; sham vs. HD, $p = 0.0018$; number of line crossing: sham vs. MD, $p = 0.0198$; sham vs. HD, $p = 0.0445$; one-way ANOVA, Tukey's multiple comparison test). In accordance, we found significant differences between LD and MD, as well as LD and HD groups of mice both in mean speed and number of line-crossings tested one week after 6-OHDA injections (average speed: LD vs. MD, $p < 0.0001$; LD vs. HD, $p < 0.0001$; number of line crossing: LD vs. MD, $p = 0.0148$; LD vs. HD, $p = 0.0389$; one-way ANOVA, Tukey's multiple comparison test). We did not find significant differences between MD and HD animals (average speed, $p = 0.9988$; number of line crossing, $p = 0.9804$; one-way ANOVA, Tukey's multiple comparison test).

Some mice were subjected to histological analysis after the tests (see below), while others were tested again in the OF arena 2 weeks after 6-OHDA injections (Fig. 2B,D). We observed a dissociation between the impact on speed of locomotion and distance covered as indexed by line-crossings. On one hand, we did not find a significant effect of the lesions on speed, however, a tendency of decrease was observed at all three doses. On the other hand, number of line-crossings showed a significant decrease in all three dose groups compared to sham-lesioned mice (sham vs. LD, $p = 0.0269$; sham vs. MD, $p = 0.0053$; sham vs. HD = 0.0011).

No rotational behavior was observed in any of the tested mice, neither one nor two weeks following drug injection.

Explorative locomotion during the first minute of the open field test

We observed that mice started to habituate to the initially new environment and move less after one minute of exploration. Therefore, to have a better insight into explorative locomotion, we performed a separate analysis of the number of line-crossings and the traveled distance during the first minute of the OF recordings (Fig. 3A,B).

We found significant differences in travelled distance when comparing sham lesioned and 6-OHDA-treated groups one week after the injections (week 1, sham vs. LD, $p < 0.0001$; sham vs. MD, $p < 0.0001$; sham vs. HD, $p < 0.0001$; one-way ANOVA, Tukey's multiple comparison test). Additionally, there was a significant difference between LD and MD groups one week following 6-OHDA injection (LD vs. MD, $p = 0.0122$; one-way ANOVA, Tukey's multiple comparison test; Fig. 3C). We found similar, albeit less pronounced effects two weeks after the injections, when the MD and HD groups significantly differed from sham-lesioned controls, and LD vs. HD groups showed a significant difference as well (week 2, sham vs. MD, $p = 0.0492$; sham vs. HD, $p = 0.0074$; LD vs HD, $p = 0.0273$; one-way ANOVA, Tukey's multiple comparison test; Fig. 3D).

When we analyzed the number of line-crossings, we found that mice in the MD and HD groups crossed significantly less mesh lines than sham lesioned animals, both one and two weeks following 6-OHDA injections (week 1, sham vs. MD, $p < 0.0001$; sham vs. HD $p < 0.0001$; week2, sham vs. MD, $p = 0.0087$; sham vs. HD, $p = 0.0003$; one-way ANOVA, Tukey's multiple comparison test; Fig. 3E,F). Mice in the LD group crossed significantly more lines than those in MD and HD groups one week post injection (LD vs. MD, $p < 0.0001$; LD vs. HD, $p < 0.0001$; one-way ANOVA, Tukey's multiple comparison test) and significantly more than those in HD groups two weeks post injection (LD v. HD, $p = 0.0115$; one-way ANOVA, Tukey's multiple comparison test). Additionally, locomotion of mice receiving low dose of 6-OHDA decreased significantly from the first week to the second week after lesion (number of line crossings: LD week 1 vs. LD week 2, $p = 0.0014$; Mann–Whitney U-test). As expected, no changes were seen in sham-lesioned mice from one to two weeks post-surgery (number of line crossings, week 1 vs. week 2, $p = 0.6840$; average speed, $p = 0.0519$).

Pauses in locomotion

We noticed that mice treated with unilateral intrastriatal 6-OHDA injections showed an increase in the number of stops during locomotion. Indeed, analyzing movement trajectories in the first one minute of the OF test revealed differences between sham lesioned and 6-OHDA treated animals. Intercepting locomotion, mice stopped for grooming, rearing, or sitting still. We defined those periods which animals spent without locomotion as 'pauses' or 'stops' if the central point of mice, defined by the Animal tracker analysis software, was localized in one cm^2 in the x–y dimension for more than two seconds. The number of pauses in all 6-OHDA treated groups showed significant differences compared to sham lesioned mice one week post injection (sham vs. LD, $p = 0.0037$; sham vs. MD, $p < 0.0001$; sham vs. HD, $p < 0.0001$; Fig. 3G). Qualitatively similar results were observed in the smaller cohorts of mice that were re-tested two weeks after the injections (Fig. 3H). While the significance of this finding is not entirely clear, the increased number of stops in 6-OHDA-injected mice may be related to bradykinesia, which is often an early symptom of Parkinson's disease and typically leads to an increase in periods of immobility in PD patients.

Motor coordination in the rotarod test

The rotarod test of motor coordination has been used as a sensitive indicator of dopaminergic cell loss in the SNc. We tested motor skills by measuring two parameters simultaneously, the latency to fall and the revolutions per minute (RPM) values at the time of fall from the rotating rod one week and two weeks after unilateral intrastriatal 6-OHDA injections.

We found no significant changes in the latency to fall and in the RPM values at the time of fall, either one week or two weeks post lesion (RPM at time of fall: week 1, sham vs. LD, $p = 0.8109$; sham vs. MD, $p = 0.9979$; sham vs. HD, $p = 0.7142$; LD vs. MD, $p = 0.8571$; LD vs. HD, p = 0.9948; MD vs. HD, $p = 0.7573$; time spend on rotarod: week 1, sham vs. LD, p = 0. 7610; sham vs. MD, $p = 0.9880$; sham vs. HD, $p = 0.6552$; LD vs. MD, $p = 0.8852$; LD vs. HD, $p = 0.9942$; MD vs. HD, $p = 0.7860$; RPM at time of fall: week 2, sham vs. LD, $p = 0.4286$; sham vs. MD, $p = 0.2582$; sham vs. HD, $p = 0.7255$; LD vs. MD, $p = 0.9552$; LD vs. HD, $p = 0.9737$; MD vs. HD, p = 0.8221; time spend on rotarod: week 2, sham vs. LD, $p = 0.4080$; sham vs. MD, $p = 0.2549$; sham vs. HD, $p = 0.7020$; LD vs. MD, $p = 0.9621$; LD vs. HD, $p = 0.9747$; MD vs. HD, $p = 0.8379$; Fig. 4). Given the concurrent marked impairments in

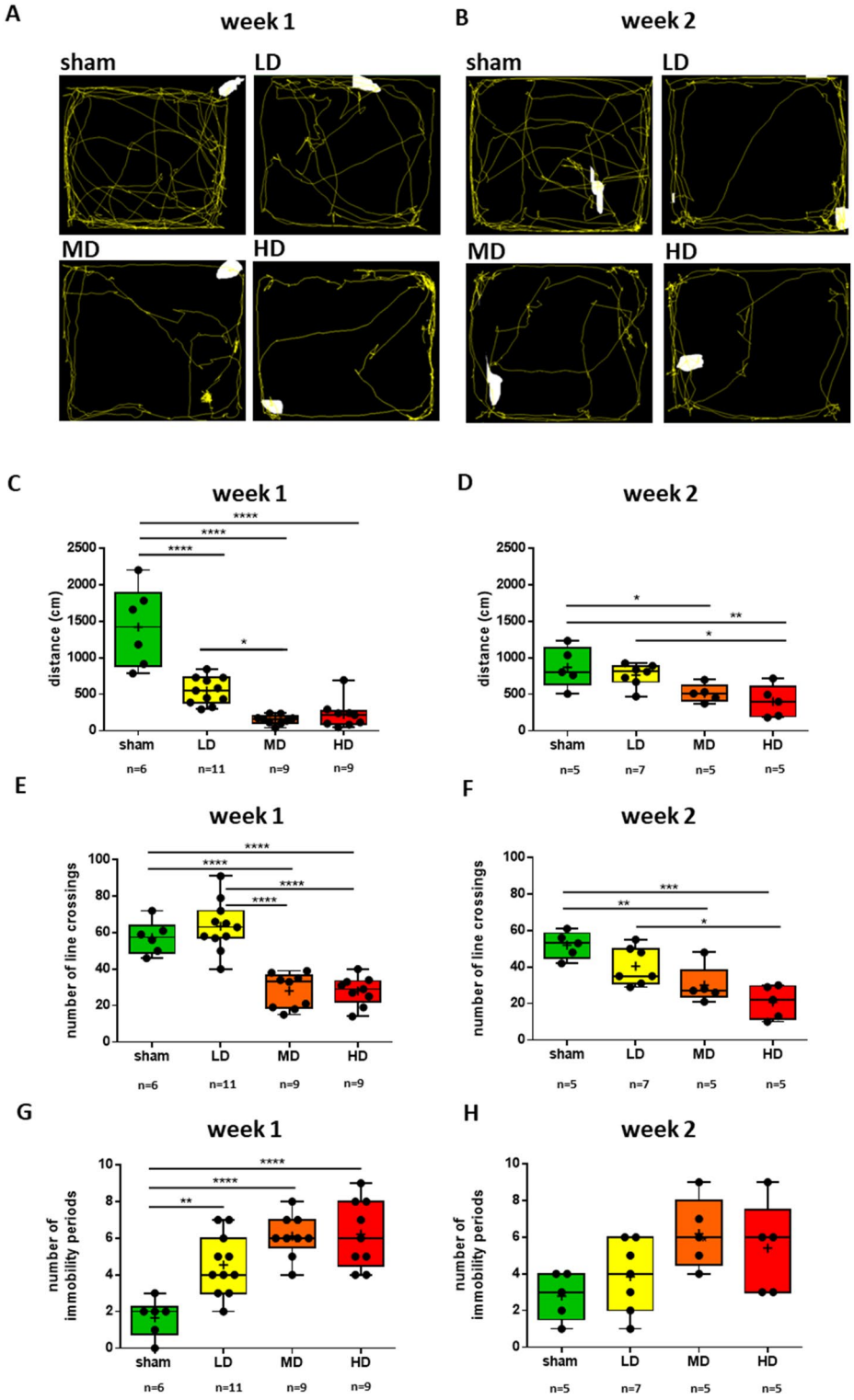

Figure 3. Explorative locomotion showed early impairment after partial unilateral striatal 6-OHDA lesion. (**A**, **B**) Representative examples of movement trajectories during the first minute of exploration in the open field test, one (**A**) and two (**B**) weeks after 6-OHDA injection. (**C**, **D**) Average distance traveled (in centimeters) during the first minute of open field exploration one (**C**) and two (**D**) weeks following 6-OHDA administration. (**E**, **F**) Number of line crossings during the first minute of open field test one week (**E**) and two weeks (**F**) following 6-OHDA administration. (**G**, **H**) Number of immobility periods during the first minute of open field test one week (**G**) and two weeks (**H**) following 6-OHDA administration. *, $p \leq 0.05$; **, $p \leq 0.01$; ***, $p \leq 0.001$; ****, $p \leq 0.0001$.

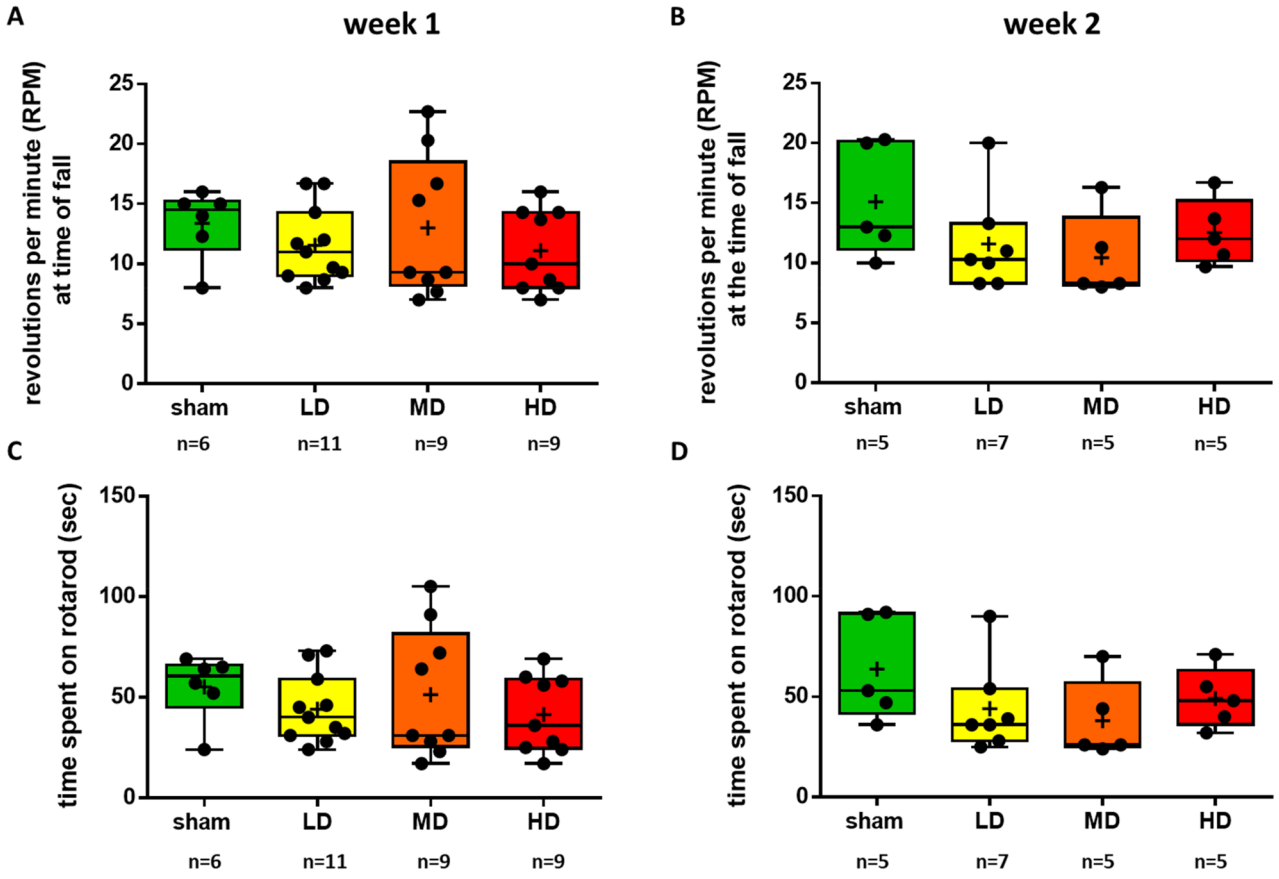

Figure 4. The rotarod test did not indicate an early impairment of motor coordination after partial unilateral striatal 6-OHDA lesion. (**A**, **B**) The average rotations per minute (RPM) at the time of fall from the rotarod one week (**A**) and 2 weeks (**B**) after partial intrastriatal lesion with different doses of 6-OHDA. (**C**, **D**) The latency to fall from the rotating rod one week (**C**) and 2 weeks (**D**) after 6-OHDA injection. LD, low dose; MD, medium dose; HD, high dose.

the OF test, this suggests a dissociation of overall horizontal locomotion and motor coordination tested short times after partial striatal 6-OHDA-mediated lesions in mice.

Histological evaluation

Quantification of dopaminergic neuronal degeneration in the SNc one and two weeks after a single unilateral intra-striatal injection of 6-OHDA

To assess the extent of tissue damage induced by our lesion protocol, we carried out a detailed histological evaluation of retrograde degeneration of DAergic neurons in the entire volume of the SNc one and two weeks after injecting 6-OHDA in the striatum unilaterally (Fig. 5). Injected hemispheres were compared with the corresponding contralateral control sides.

We found significant neurodegeneration of DAergic neurons of the SNc following 6-OHDA injection, which was apparent already after the low-dose injection. The extent of dopaminergic cell loss was similar when assessed one vs. two weeks post injection surgery, demonstrating a definitive early-stage damage (mean values of number of TH + neurons in percentage compared to control side, week1, sham, 96.58; LD, 67.43; MD, 64.93; HD, 53.66; week 2, sham, 97.57; LD, 61.07; MD, 55.84; HD, 52.55; statistical comparisons, week1, sham vs. LD, $p < 0.0001$, sham vs. MD, $p < 0.0001$, sham vs. HD, $p < 0.0001$, LD vs. MD, $p = 0.9425$, LD vs. HD, $p = 0.0099$, MD vs. HD, $p = 0.0615$; week2, sham vs. LD, $p < 0.0001$, sham vs. MD, $p < 0.0001$, sham vs. HD, $p < 0.0001$, LD vs. MD, $p = 0.7165$, LD vs. HD, $p = 0.3105$, MD vs. HD, $p = 0.9101$; Fig. 5B,C).

Quantification of dopaminergic neuronal degeneration at three different anteroposterior levels one and two weeks after a single unilateral intra-striatal injection of 6-OHDA

In order to characterize whether the different anteroposterior (AP) levels of the SNc were differentially affected by DAergic neurodegeneration, we examined whether neuronal cell loss was present at distinct AP levels of the SNc. The entire SNc was divided into three consecutive anteroposterior subregions corresponding to three ranges of AP levels (range 1, 2.54–2.92 mm; range 2, 2.92–3.52 mm; range 3, 3.52–3.80 mm; Fig. 5). We quantified and compared the extent of DAergic neuronal loss induced by different 6-OHDA concentrations, and after different survival times at these three different anteroposterior levels. (Fig. 5D–I).

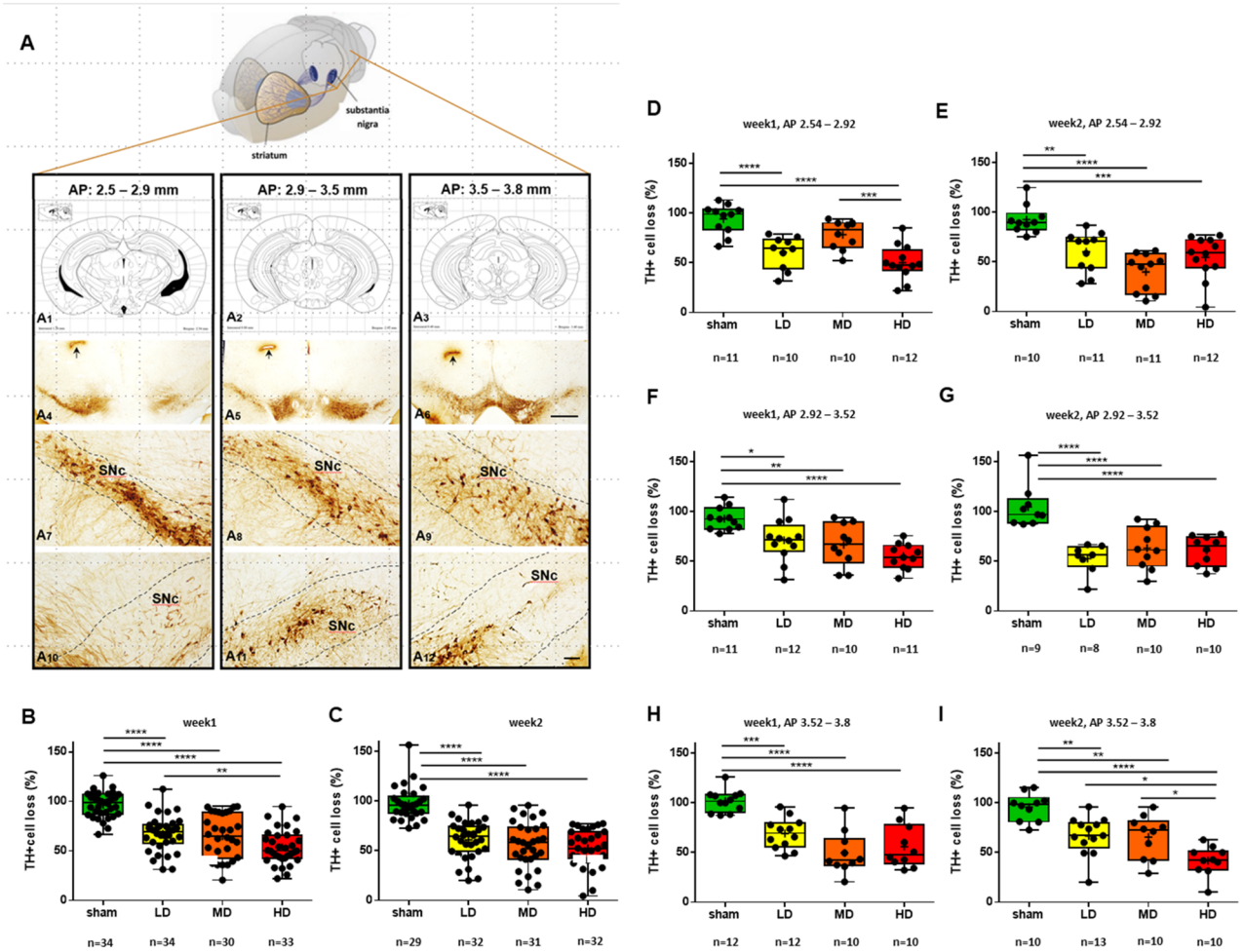

Figure 5. Quantification of the dopaminergic cell loss in the substantia nigra after partial unilateral striatal 6-OHDA lesion. (**A**) The three columns represent the chosen anteroposterior levels of the mouse brain in which TH + neurons were quantified. A_1–A_3, Anteroposterior ranges were selected on the basis of the Paxinos and Watson and Paxinos and Franklin atlases (range 1, AP 2.54–2.92 mm; range 2, 2.92–3.52 mm; range 3, 3.52–3.80 mm relative to Bregma). A_4–A_6, Bright field images showing DAB labelling of TH + DAergic neurons of the substantia nigra at the three selected AP levels. Black arrows indicate tissue marks made after perfusion to label the lesioned hemisphere. A_7–A_9, Intact TH labelling in the substantia nigra of the control hemisphere. A_{10}–A_{12}, Loss of TH + DAergic neurons on the lesioned side 2 weeks following high dose 6-OHDA injection. (**B**, **C**) The percentage of TH + DAergic neurons in the substantia nigra relative to the contralateral side 1 week (**B**) and 2 weeks (**C**) following unilateral intra-striatal 6-OHDA injection. N = 4 animals per group. Each dot represents a distinct field of view. (**D**, **E**) The percentage of TH + DAergic neurons in the substantia nigra relative to the contralateral side one week (**D**) and two weeks (**E**) following unilateral intra-striatal 6-OHDA injection quantified in the 2.54 – 2.92 mm AP range. (**F**, **G**) The percentage of TH + DAergic neurons in the substantia nigra relative to the contralateral side one week (**F**) and two weeks (**G**) following unilateral intra-striatal 6-OHDA injection quantified in the 2.92–3.52 mm AP range. (**H**, **I**) The percentage of TH + DAergic neurons in the substantia nigra relative to the contralateral side 1 week (**H**) and 2 weeks (**I**) following unilateral intra-striatal 6-OHDA injection quantified in the 3.52–3.8 mm AP range. N = 4 animals per group. Scale bar for A_4–A_6, 500 µm; for A_7–A_{12}, 100 µm. *, $p \leq 0.05$; **, $p \leq 0.01$; ***, $p \leq 0.001$; ****, $p \leq 0.0001$. The figure was created with BioRender.com. Copyright with permission from Elsevier.

When tested one week after injections, we observed a dose-dependent effect of 6-OHDA on SNc DAergic neurons (week 1, AP 2.54–2.92: means: sham, 94.32; LD, 60.57; MD, 78.40; HD, 50.26; statistical comparisons: sham vs. LD, $p = 0.0001$; sham vs. MD, $p = 0.1183$; sham vs. HD, $p < 0.0001$; LD vs. MD, $p = 0.0747$; LD vs. HD, $p = 0.4402$; MD vs. HD, $p = 0.0010$; AP 2.92–3.52: means: sham, 93.15; LD, 71.37; MD, 66.73; HD, 55.20; statistical comparisons: sham vs. LD, $p = 0.0226$; sham vs. MD, $p = 0.0064$; sham vs. HD, $p < 0.0001$; LD vs. MD, $p = 0.9236$; LD vs. HD, $p = 0.1317$; MD vs. HD, $p = 0.4345$; AP 3.54–3.80: means: sham, 101.8; LD, 69.21; MD, 49.65; HD, 56.06; statistical comparisons: sham vs. LD, $p = 0.0003$; sham vs. MD, $p < 0.0001$; sham vs. HD, $p < 0.0001$; LD vs. MD, $p = 0.0600$; LD vs. HD, $p = 0.3124$; MD vs. HD, $p = 0.8469$).

We observed pronounced DAergic neuronal loss at all three AP levels, with all three injection doses when tested two weeks after 6-OHDA injections (Fig. 5B–I). Mice injected with high dose showed significantly less

remaining DAergic cells at the posterior-most AP level compared to both the LD and MD group, indicating dose-dependent retrograde DAergic degeneration (week 2, AP 2.54–2.92: means: sham, 92.73; LD, 60.35; MD, 40.05; HD, 54.67; statistical comparisons: sham vs. LD, $p = 0.0021$; sham vs. MD, $p < 0.0001$; sham vs. HD, $p = 0.0002$; LD vs. MD, $p = 0.0772$; LD vs. HD, $p = 0.8918$; MD vs. HD, $p = 0.2745$; AP 2.92–3.52: means: sham, 104.9; LD, 52.91; MD, 63.35; HD, 60.69; statistical comparisons: sham vs. LD, $p < 0.0001$; sham vs. MD, $p = 0.0001$; sham vs. HD, $p < 0.0001$; LD vs. MD, $p = 0.6377$; LD vs. HD, $p = 0.8118$; MD vs. HD, $p = 0.9883$; AP 3.54–3.80: means: sham, 95.77; LD, 66.70; MD, 65.70; HD, 41.86; statistical comparisons: sham vs. LD, $p = 0.0023$; sham vs. MD, $p = 0.0031$; sham vs. HD, $p < 0.0001$; LD vs. MD, $p = 0.9992$; LD vs. HD, $p = 0.0108$; MD vs. HD, $p = 0.0248$).

Qualitative analysis of ultrastructural changes in dopaminergic neurons

The precise mechanisms underlying neuronal injury in PD are not yet fully elucidated; however, previous studies suggested that early changes in neuronal ultrastructure of midbrain dopaminergic neurons play a key role in the pathogenesis[49–53]. Therefore, we examined the morphological features of dopaminergic neurons in tissue samples from the SNc and the striatum by electron microscopy. Dopaminergic neurons were labeled by TH immunohistochemistry using DAB as chromogen. Pre-embedding immunogold labeling combined with a second immunoperoxidase staining was used to examine the ultrastructural changes of the degenerating DAergic neurons in the SNc.

The cellular ultrastructure of TH + neurons showed morphological alterations in 6-OHDA treated mice (Fig. 6). Specifically, by qualitative electron microscopic analysis, vacuoles in dendrites and axons of TH-expressing DAergic neurons were found. Additionally, swollen and vacuolized dopaminergic axons were seen in the striatum, and swollen, vacuolized mitochondria were found in the somata and proximal dendrites of the

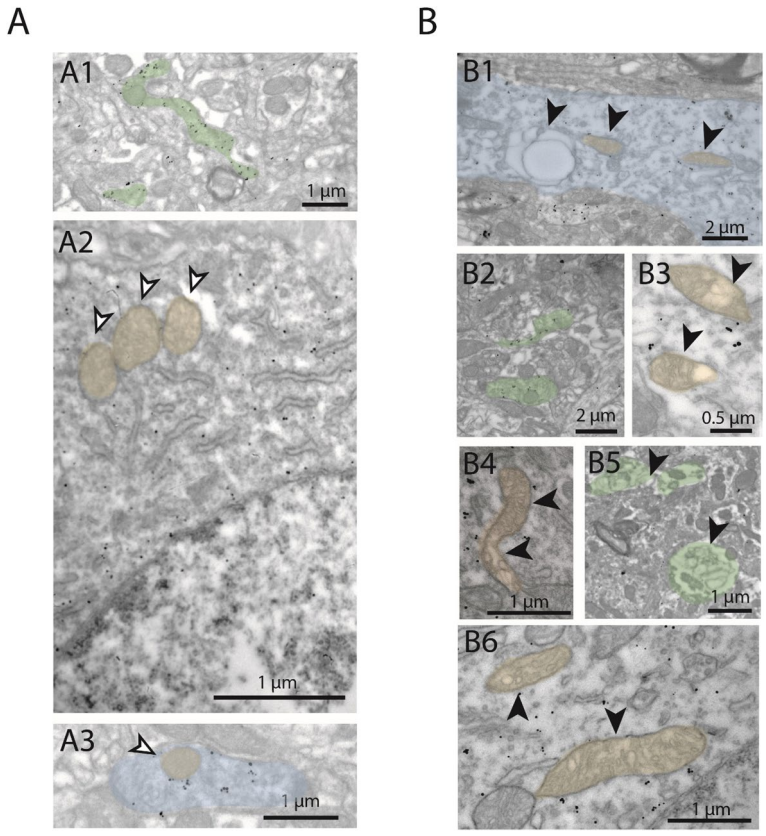

Figure 6. Subcellular morphological changes of dopaminergic neurons one and two weeks after striatal high-dose 6-OHDA injection. (**A**) In sham control animals, no morphological changes were observed in the subcellular structures of SNc dopaminergic neurons in their preterminal axon segment in the striatum (A1, green), the mitochondria in their somata (A2, orange), or in their dendrites (A3, blue). Gold particles are indicating the presence of TH (immunogold staining). Note the intact inner lamellar structures of mitochondria. (**B**) Subcellular signs of neurodegeneration were found in the injected hemisphere of 6-OHDA-injected mice. B1–B3, One week after intrastriatal 6-OHDA injection. B1, Swollen, vacuolized (black arrowhead, left) dopaminergic dendrite (blue) in the SNc. B2, Moderately swollen axons (green) in the striatum. B3, Vacuolized mitochondria (orange) in the soma of a dopaminergic SNc neuron. B4-B6, 2 weeks after intrastriatal 6-OHDA injection. B4 and B6, Vacuolized, desintegrating mitochondria (orange) in the soma of a dopaminergic SNc neuron on the 6-OHDA-injected side. B5, Axons (green) in the striatum showing signs of neurodeneration (lamellar body formation). White arrowheads: healthy structures; black arrowheads: structures with signs of neurodegeneration.

gold-labeled dopaminergic neurons. Signs of neurodegeneration were present already one week following the 6-OHDA injection. Two weeks following surgery, signs of a prominent neurodegeneration were observed, including mitochondria with disintegrated membranes, as well as deformed and disintegrated dopaminergic cell bodies.

Discussion

Early stages of PD were studied in a graded 6-OHDA mouse model to explore early motor symptoms and associated histological conditions at the cellular and ultrastructural level. Loss of tyrosine-hydroxylase-expressing DAergic cells and neural ultrastructural changes were characterized. Explorative behavior and motor impairments were tested by open field and rotarod behavioral assays. Our results show that mild motor impairments, characterized by a dissociation of explorative horizontal locomotion in open field (impaired) and motor coordination on the rotarod (intact), are detectable already at very early stages, even one week after a single low dose of striatal 6-OHDA injection.

PD leads to severe motor symptoms: tremor, rigidity, bradykinesia and postural instability[54–57] as well as non-motor symptoms including depression and altered motivation, autonomic dysfunction such as constipation and bladder dysfunction, sleep disturbances, anosmia and cognitive deficit[58–61]. The key component of PD pathogenesis is the degeneration of DAergic neurons of the SNc, resulting in the deafferentation of the striatum[7,62]. The onset of cellular neurodegenerative mechanisms underlying PD precedes the appearance of the disease symptoms by multiple years[12,57,63]: estimations date the initial presymptomatic phase 5 to 30 years prior to the clinical manifestation[6]. Motor symptoms first appear in patients after the degeneration of 50–60% of DAergic neurons and 70–80% dopamine depletion in the striatum[55–57,64].

Most animal models represent an advanced phase of the disease, with substantial DAergic cell loss resulting in severe motor deficit[65]. However, a better understanding of the early phase of PD could lead to efficient ways of early detection and intervention, potentially leading to more efficient therapeutical options. Accordingly, there is an increasing number of recent studies on the early stages of PD[14,15,17,18]; nevertheless, this aspect of the disease requires further attention. Therefore, to better understand the processes which lead to the final neuronal degeneration of the dopaminergic system in SNc, we focused on the early events of PD genesis. We examined the early changes associated with PD in a graded-dose 6-OHDA mouse model, where slight early motor impairments were correlated with mild neurodegeneration and neuronal ultrastructural changes in dopaminergic neurons. Our results show that mild ultrastructural and cellular degradation of DAergic neurons can lead to certain motor deficits in the early stage of the disease.

A growing number of human studies have highlighted the importance of studying the early phases of PD[11]. For instance, one study found that α-synuclein levels in the cerebrospinal fluid decrease relatively early in PD, while its concentrations do not correlate with PD progression, thus emphasizing the need for more direct early-onset biomarkers[17]. Another paper examined newly diagnosed PD patients with mild cognitive impairment using fMRI, and found disrupted functional connectivity in patients[13]. An elegant study by Mallet et al. investigated 6-OHDA-injected rats, an α-synuclein rat model, an MPTP monkey model as well as de novo PD patients corresponding to different stages of the disease, and suggested a serum biomarker composed of six metabolites based on the results[18].

These human studies call for robust and high throughput animal models of the prodromal phase of PD to realize an efficient search for early biomarkers, allow investigation of causative disease pathomechanisms and provide a testing platform for proposed therapies. Toxin models achieved by intracerebral 6-OHDA injections represent a popular and powerful tool to model pathologies associated with PD. A recent line of studies used partial bilateral lesions of the midbrain DAergic system in rats to test PD-associated early non-motor impairments. Drui et al. demonstrated that selective lesions to the SNc leads to isolated motivational deficits and affective impairments[14], while later studies revealed an underlying D3 dopamine receptor dependent mechanism[15,66].

However, most studies investigating early PD used rats, likely due to their classical role in studying the building blocks of mammalian behavior[65,67], whereas advancements in genetic tools for mice as well as their more affordable husbandry shifted rodent research towards an increasing focus on mice. Nevertheless, investigating PD models in mice has been less frequent and full-fledged 6-OHDA PD models for mice are still being developed. Therefore, unlike most previous studies on early PD, we decided to focus on mice.

Injections delivered in the SNc or MFB typically result in rapid degeneration of DAergic neurons that starts as early as 24 h within the surgery, leading to an 80% loss of DAergic neurons in 3–4 days and a complete degeneration in 3 weeks[65,67,68]. Dose-dependent behavioral impairments and DAergic loss of neurons and fibers were demonstrated in rats following intrastriatal injections, proposing the protocol as a suitable approach to investigate early stages of PD and to test potentially preventive interventions[69,70]; however, unilateral intrastriatal lesions are comparably less studied in mice. Therefore, to avoid a rapid and complete lesion of SNc DAergic neurons, we performed unilateral intra-striatal 6-OHDA injections at three different doses, with even the highest applied dose being relatively moderate. A recent line of elegant studies focusing on L-DOPA induced dyskinesia has suggested that this approach might be applicable for studying PD in mice as well[71–74]. Unlike most other studies, we tested mice as early as one and two weeks post lesion, demonstrating that unilateral intrastriatal graded-dose 6-OHDA injections lead to early onset dose-dependent motor deficits. We suggest that future studies should explore early signs of PD-associated non-motor symptoms in this model.

The rotarod test is widely used in rodent PD models for assessing deficits of motor coordination in rodents with bilateral[30] or unilateral[75,76] lesions[65] and a correlation between DAergic cell loss and time spent on the rotarod has been demonstrated in both rat and mouse 6-OHDA models[75,77]. Surprisingly, we did not find any early deficits in rotarod performance after applying our partial lesion protocol, either in RPM at the time of fall or in latency to fall, despite the presence of DAergic degeneration. However, by careful reassessment of previous results, it appears that the strong correlation between lesion extent and rotarod performance is mostly driven by

a dramatic performance drop at > 80% cell loss, whereas the correlation is not obvious when considering cases with < 80% cell loss, and likely not present for cases with < 70% cell loss (see Fig. 5. in ref[75]). Therefore, although the rotarod test is regarded as a sensitive indicator of DAergic degeneration in the SNc, our results suggest that it may not serve as a good marker for early deficits in rodent PD. Therefore, we propose that stepping tests, considered sensitive in unilateral lesion models, may also be tested.

Although the rotarod test did not indicate an early impairment in motor coordination, motor deficits were detectable as a decrease in overall horizontal locomotion in the open field arena. Rats receiving unilateral 6-OHDA injections in the MFB[76], SNc[28] or striatum[78] were shown to be impaired in open field locomotion. While less studied in mice, a recent study showed similar results in a unilateral intrastriatal mouse model[77]. On one hand, our results confirmed these earlier studies. On the other hand, the early dose-dependent impairment of horizontal locomotion that was observed in the absence of a concurrent impairment in rotarod performance indicates that the OF test may be a sensitive measure of early-stage impairment in PD mouse models. This locomotion impairment was most pronounced when we focused on exploratory locomotion in the first minute of the OF test, in line with some earlier studies showing impaired exploratory behavior in rat PD models[79]. Medium and high dose injections led to a significant decrease in the number of line crossings already when tested one week post injection, while mice injected with the lowest dose applied appeared to develop similar impairments by the second week after the surgery, shedding light on the dose-dependent time course of the early locomotion impairment.

We noticed that movement was often interrupted by grooming, rearing, or simply staying still in lesioned mice, which we defined as 'pauses' and quantified. This increased fragmentation of behavior may be related to problems with movement initiation and/or execution of a motor plan[80,81]. However, such interruptions in locomotion have not been typically associated with PD, and therefore their exact significance should be determined by future studies. It is nonetheless possible, that this phenotype is an early sign of motor deficit in PD models, that may later be masked by more severe motor impairments during disease progression.

In parallel with the behavioral characterization, we also evaluated the structural degeneration of SNc DAergic neurons by histological and electron microscopy techniques. We observed a significant loss of SNc DAergic neurons already one week after drug injection, which did not show obvious further worsening when tested two weeks post surgery. We showed by electron microscopy that DAergic neurons developed early signs of neurodegeneration, which can probably lead to neural cell death. The functional DAergic deficit may lead to network dysfunctions, which could accelerate disease progression[82], resulting in earlier cell death, as well as the emergence or worsening of clinical symptoms. Intervention should target those DAergic neurons still viable, possibly by activating neuroprotective mechanisms to slow or stop disease progression[81,83,84].

The relatively intact horizontal locomotion one week after injecting the lowest dose of 6-OHDA with cell death already present in the SNc suggests there was no one-to-one correspondence of DAergic cell counts and motor function, for which multiple explanations are plausible. First, cell loss without functional deficit was observed in prodromal stages, probably due to both reserve capacities of the remaining neuronal populations but also because of compensatory changes. These compensatory changes can likely be exhausted without substantial further cell loss[19,85,86]. It is possible that such compensation underlies the relatively preserved locomotor functions one week post lesion using low doses of 6-OHDA, while these mechanisms cannot cope with higher doses as well as break down by the second week post lesion.

Second, functional deficits without cell death have already been demonstrated in some studies[87]. Specifically, dopamine release was found impaired before the appearance of cell loss. PET imaging studies in humans suggested a presynaptic dopaminergic dysfunction as one of the early events in PD pathophysiology, indicated by a reduced ^{18}F-DOPA uptake[88,89]. Thus, it is also conceivable that widespread functional deficits make some conditions worse than others even at similar DAergic cell counts, e.g. between mice injected with low dose and higher doses of 6-OHDA, or from the first to the second week post 6-OHDA injection.

These functional deficits have been studied in humans and genetic animal models; however, the otherwise powerful toxin models were not appropriate for these studies due to the rapid loss of neurons[88]. Our study may start filling this gap by introducing a controlled, mild and gradual toxin model that allows the investigation of early functional changes of dopamine release, e.g. by using the recently developed fluorescent DA sensors[90].

One suggested mechanism involves the downregulation of the GABA uptake transporters in striatal astrocytes, leading to an enhanced GABAergic inhibition of DA release[47,91]. However, impaired exocytosis due to decreased mitochondrial function in DAergic neurons has also been detected[92,93]. Additionally, vesicle loading requires an ATP-dependent pH gradient also dependent on intact mitochondrial respiratory chain[94]. Noting one caveat, as with every animal model, 6-OHDA models may reproduce some aspects of the pathology more than others; e.g. in this context, based on the mitochondrial mechanisms of 6-OHDA[95], functional impairment of DA release is more expected based on the mitochondrial energy deficit than the astrocytic mechanism. This has to be elucidated by future studies and emphasizes the need for multiple approaches of animal models when investigating human disease pathophysiology.

In addition, axonal degeneration may precede cell loss in PD patients[96]. This may actually be mimicked by retrograde axonal degeneration following intrastriatal 6-OHDA injections[97,98]. We also found that ultrastructural degenerations were present already one week following 6-OHDA injections in TH-immunopositive dopaminergic neurons, e.g. swollen and vacuolized organelles. This result suggests that functionally damaged DAergic neurons may occur with TH-immunopositive somata still present and thus contributing to the cell counts assessed by light microscopy. Thus, functional and ultrastructural impairments might be manifested in motor and non-motor deficits even with comparable midbrain DAergic populations.

Our data showed that an impairment of locomotion can be observed already one week following unilateral intrastriatal 6OHDA injection, likely in consequence of the significant decrease of SNc DAergic neurons and the ultrastructural neurodegeneration already present at that time. Studies in rats found differences in several

gait parameters as early as one week following striatal 6-OHDA lesion accompanied by mild TH + neural loss[99]. Our partial 6-OHDA mouse model provides a useful tool to examine the early phase of PD, featuring mild early deficits with progressive characteristics, described here at the ultrastructural, histopathological, and behavioral levels. We think that models that enable studying the early phases of neurodegeneration can provide important tools to test neuroprotective strategies in animal models that might pave the way towards novel therapeutic interventions in patients with PD[100].

Conclusion

Due to the complex etiology of PD, its pathogenesis has not yet been fully elucidated. It is widely held that PD is a progressive and deteriorating polycentric neurodegenerative disease associated with neurotransmitter systems[62,101]. One main pathological mechanism of PD is the gradual degeneration and loss of DAergic neurons in the substantia nigra pars compacta, resulting in the lack of neurotransmitter DA in the basal ganglia system[102]. Neuroprotective intervention is possible at the early stage of PD when more of the DAergic neurons and fibers remain intact. In the early stage of the disease, a targeted treatment could possibly prevent or stop the degeneration of dopaminergic neurons.

6-OHDA-mediated lesion models in rodents can be used to model distinct stages of the human pathology by varying the localization and the extent of the lesion[65,77]. Partial lesions of the nigrostriatal dopaminergic system might be considered analogous to the early stages of human Parkinson's disease and can be induced reliably by intrastriatal injections of 6-OHDA. Therefore, we used this model to characterize the early signs of neurodegeneration, at which stage possible interventions might be more efficient. We described the morphological and behavioral alterations in this mouse model that may aid the quest for early diagnosis and treatment.

Data availability

The datasets used and/or analyzed during the current study are available from the corresponding author on reasonable request.

Received: 15 March 2023; Accepted: 2 November 2023
Published online: 09 November 2023

References

1. Obeso, J. A. *et al.* Past, present, and future of Parkinson's disease: A special essay on the 200th Anniversary of the Shaking Palsy. *Mov. Disord.* **32**, 1264–1310 (2017).
2. Przedborski, S. The two-century journey of Parkinson disease research. *Nat. Rev. Neurosci.* **18**, 251–259 (2017).
3. Bloem, B. R., Okun, M. S. & Klein, C. Parkinson's disease. *Lancet* **397**, 2284–2303 (2021).
4. Jankovic, J. & Aguilar, L. G. Current approaches to the treatment of Parkinson's disease. *Neuropsychiatr. Dis. Treat.* **4**, 743–757 (2008).
5. Schapira, A. H. V., Chaudhuri, K. R. & Jenner, P. Non-motor features of Parkinson disease. *Nat. Rev. Neurosci.* **18**, 435–450 (2017).
6. Fearnley, J. M. & Lees, A. J. Ageing and parkinson's disease: Substantia nigra regional selectivity. *Brain* **114**, 2283–2301 (1991).
7. Ehringer, H. & Hornykiewicz, O. Verteilung Von Noradrenalin Und Dopamin (3-Hydroxytyramin) Im Gehirn Des Menschen Und Ihr Verhalten Bei Erkrankungen Des Extrapyramidalen Systems. *Klin. Wochenschr.* **38**, 1236–1239 (1960).
8. Dawson, V. L. & Dawson, T. M. Promising disease-modifying therapies for Parkinson's disease. *Sci. Transl. Med.* **11**, 1–4 (2019).
9. Braak, H., Rüb, U., Gai, W. P. & Del Tredici, K. Idiopathic Parkinson's disease: Possible routes by which vulnerable neuronal types may be subject to neuroinvasion by an unknown pathogen. *J. Neural Transm.* **110**, 517–536 (2003).
10. Fahn, S. Description of Parkinson's disease as a clinical syndrome. *New York Acad. Sci.* **991**, 1–14 (2003).
11. Rodriguez-Oroz, M. C. *et al.* Initial clinical manifestations of Parkinson's disease: Features and pathophysiological mechanisms. *Lancet Neurol.* **8**, 1128–1139 (2009).
12. Li, J. *et al.* Alterations of regional homogeneity in the mild and moderate stages of Parkinson's disease. *Front. Aging Neurosci.* **13**, 1–10 (2021).
13. Chen, X., Liu, M., Wu, Z. & Cheng, H. Topological abnormalities of functional brain network in early-stage Parkinson's disease patients with mild cognitive impairment. *Front. Neurosci.* **14**, 1–7 (2020).
14. Drui, G. *et al.* Loss of dopaminergic nigrostriatal neurons accounts for the motivational and affective deficits in Parkinson's disease. *Mol. Psychiatry* **19**, 358–367 (2014).
15. Favier, M. *et al.* Pramipexole reverses Parkinson's disease-related motivational deficits in rats. *Mov. Disord.* **29**, 912–920 (2014).
16. Graham, S. F. *et al.* Metabolomic profiling of bile acids in an experimental model of prodromal parkinson's disease. *Metabolites* **8**, 71–80 (2018).
17. Mollenhauer, B. *et al.* Longitudinal analyses of cerebrospinal fluid α-Synuclein in prodromal and early Parkinson's disease. *Mov. Disord.* **34**, 1354–1364 (2019).
18. Mallet, D. *et al.* A metabolic biomarker predicts Parkinson's disease at the early stages in patients and animal models. *J. Clin. Invest.* **132**, 1–16 (2022).
19. Mahlknecht, P., Seppi, K. & Poewe, W. The concept of prodromal Parkinson's disease. *J. Parkinsons. Dis.* **5**, 681–697 (2015).
20. Dunnett, S. B. & Lelos, M. Behavioral analysis of motor and non-motor symptoms in rodent models of Parkinson's disease. *Prog. Brain Res.* **184**, 35–51 (2010).
21. Hou, J. G. G. & Lai, E. C. Non-motor symptoms of Parkinson's disease. *Int. J. Gerontol.* **1**, 53–64 (2007).
22. Chu, H. Y., McIver, E. L., Kovaleski, R. F., Atherton, J. F. & Bevan, M. D. Loss of hyperdirect pathway cortico-subthalamic inputs following degeneration of midbrain dopamine neurons. *Neuron* **95**, 1306–1318 (2017).
23. van Wijk, B. C. M. Is broadband gamma activity pathologically synchronized to the beta rhythm in parkinson's disease?. *J. Neurosci.* **37**, 9347–9349 (2017).
24. Przedbroski, S. *et al.* Dose-dependent lesions of the dopaminergic nigrostriatal pathway induced by instrastriatal injection of 6-hydroxydopamine. *Neuroscience* **67**, 631–647 (1995).
25. Park, S. E., Song, K. I., Kim, H., Chung, S. & Youn, I. Graded 6-OHDA-induced dopamine depletion in the nigrostriatal pathway evokes progressive pathological neuronal activities in the subthalamic nucleus of a hemi-parkinsonian mouse. *Behav. Brain Res.* **344**, 42–47 (2018).
26. Iarkov, A., Barreto, G. E., Grizzell, J. A. & Echeverria, V. Strategies for the treatment of Parkinson's disease: Beyond dopamine. *Front. Aging Neurosci.* **12**, 1–20 (2020).

27. Cenci, M. A. & Lundblad, M. Ratings of L-DOPA-induced dyskinesia in the unilateral 6-OHDA lesion model of parkinson's disease in rats and mice. *Curr. Protoc. Neurosci.* **41**, 1–23 (2007).
28. Steiner, H. & Kitai, S. T. Unilateral striatal dopamine depletion: Time-dependent effects on cortical function and behavioural correlates. *Eur. J. Neurosci.* **14**, 1390–1404 (2001).
29. Tadaiesky, M. T. & Dombrowski, P. A. Emotinal, cognitive and neurochemical alterations in a premotor stage model of Parkinson's disease. *Neuroscience* **156**, 830–840 (2008).
30. Campos, F. L. *et al.* Rodent models of Parkinson's disease: Beyond the motor symptomatology. *Front. Behav. Neurosci.* **7**, 1–11 (2013).
31. Soler, R., Fullhase, C. & Santos, C. A. Suppression of bladder overactivity by adenosine A 2A receptor antagonist in a rat model of Parkinson's disease. *J. Urol.* **183**, 1–2 (2010).
32. Yoshimura, N., Kuno, S., Chancellor, M. B., de Groat, W. C. & Seki, S. Dopaminergic mechanisms underlying bladder hyperactivity in rats with a unilateral 6-hydroxydopamine (6-OHDA) lesion of the nigrostriatal pathway. *Br. J. Pharmacol.* **139**, 1425–1432 (2003).
33. Karasawa, H. *et al.* New ghrelin agonist, HM01 alleviates constipation and L-dopa-delayed gastric emptying in 6-hydroxydopamine rat model of Parkinson's disease. *Neurogastroenterol. Motil.* **26**, 1771–1782 (2014).
34. Paxinos, G. & Watson, C. *Chemoarchitectonic Atlas of the Mouse Brain* (Academic Press, 2010).
35. Paxinos, G. & Franklin, K. B. J. *The Mouse Brain in Stereotaxic Coordinates* (Elsevier, 2003).
36. Franklin, M. A., Keith, B. J. & Paxinos, G. *The Mouse Brain in Stereotaxic Coordinates* (Elsevier, 2008).
37. Gulyás, M., Bencsik, N., Pusztai, S., Liliom, H. & Schlett, K. AnimalTracker: An ImageJ-based tracking API to create a customized behaviour analyser program. *Neuroinformatics* **14**, 479–481 (2016).
38. Mátyás, F. *et al.* Identification of the sites of 2-arachidonoylglycerol synthesis and action imply retrograde endocannabinoid signaling at both GABAergic and glutamatergic synapses in the ventral tegmental area. *Neuropharmacology* **54**, 95–107 (2008).
39. Bartho, P. *et al.* Cortical control of Zona incerta. *J. Neurosci.* **27**, 1670–1681 (2007).
40. Barthó, P. *et al.* Ongoing network state controls the length of sleep spindles via inhibitory activity. *Neuron* **82**, 1367–1379 (2014).
41. Bokor, H. *et al.* Selective GABAergic control of higher-order thalamic relays. *Neuron* **45**, 929–940 (2005).
42. Slezia, A. *et al.* Phase advancement and nucleus-specific timing of thalamocortical activity during slow cortical oscillation. *J. Neurosci.* **31**, 607–617 (2011).
43. Proctor, C. M. *et al.* Electrophoretic drug delivery for seizure control. *Sci. Adv.* **4**, 1–8 (2018).
44. Slezia, A., Proctor, C. M., Kaszas, A., Malliaras, G. G. & Williamson, A. Electrophoretic delivery of γ-aminobutyric acid (GABA) into epileptic focus prevents seizures in mice. *J. Vis. Exp.* **147**, 1–9 (2019).
45. Kaszas, A. *et al.* Two-photon GCaMP6f imaging of infrared neural stimulation evoked calcium signals in mouse cortical neurons in vivo. *Sci. Rep.* **11**, 1–18 (2021).
46. Varga, V. *et al.* The presence of pacemaker HCN channels identifies theta rhythmic GABAergic neurons in the medial septum. *J. Physiol.* **586**, 3893–3915 (2008).
47. Rice, M. W., Roberts, R. C., Melendez-Ferro, M. & Perez-Costas, E. Mapping dopaminergic deficiencies in the substantia nigra/ventral tegmental area in schizophrenia. *Brain Struct. Funct.* **221**, 185–201 (2016).
48. Melendez-Ferro, M., Rice, M. W., Roberts, R. C. & Perez-Costas, E. An accurate method for the quantification of cytochrome C oxidase in tissue sections. *J. Neurosci. Methods* **214**, 156–162 (2013).
49. Park, J. H. *et al.* Alpha-synuclein-induced mitochondrial dysfunction is mediated via a sirtuin 3-dependent pathway. *Mol. Neurodegener.* **15**, 1–19 (2020).
50. Perier, C. & Vila, M. Mitochondrial biology and Parkinson's disease. *Cold Spring Harb. Perspect. Med.* **2**, 1–19 (2012).
51. Öztürk, Z., O'Kane, C. J. & Pérez-Moreno, J. J. Axonal endoplasmic reticulum dynamics and its roles in neurodegeneration. *Front. Neurosci.* **14**, 1–33 (2020).
52. Burté, F., Carelli, V., Chinnery, P. F. & Yu-Wai-Man, P. Disturbed mitochondrial dynamics and neurodegenerative disorders. *Nat. Rev. Neurol.* **11**, 11–24 (2015).
53. Park, J.-S., Davis, R. L. & Sue, C. M. Mitochondrial dysfunction in Parkinson's disease: New mechanistic insights and therapeutic perspectives. *Curr. Neurol. Neurosci. Rep.* **18**, 21 (2018).
54. Fahn, S. The history of dopamine and levodopa in the treatment of Parkinson's disease. *Mov. Disord.* **23**, S497–S508 (2008).
55. Agid, Y. Parkinson' s disease: Pathophysiology. *Lancet* **337**, 1321–1324 (1991).
56. Bernheimer, H., Birkmayer, W., Hornykiewicz, O., Jellinger, K. & Seitelberger, F. Brain dopamine and the syndromes of Parkinson and Huntington Clinical, morphological and neurochemical correlations. *J. Neurol. Sci.* **20**, 415–455 (1973).
57. Riederer, P. & Wuketich, S. Time course of nigrostriatal degeneration in Parkinson's disease—A detailed study of influential factors in human brain amine analysis. *J. Neural Transm.* **38**, 277–301 (1976).
58. Schapira, A. H. V., Olanow, C. W., Greenamyre, J. T. & Bezard, E. Slowing of neurodegeneration in Parkinson's disease and Huntington's disease: Future therapeutic perspectives. *Lancet* **384**, 545–555 (2014).
59. French, I. T. & Muthusamy, K. A. A review of sleep and its disorders in patients with Parkinson's disease in relation to various brain structures. *Front. Aging Neurosci.* **8**, 1–20 (2016).
60. Titova, N. & Chaudhuri, K. R. Personalized medicine and nonmotor symptoms in Parkinson's disease. *Int. Rev. Neurobiol.* **134**, 1257–1281 (2017).
61. Johnson, M. E., Stecher, B., Labrie, V., Brundin, L. & Brundin, P. Triggers, facilitators, and aggravators: Redefining Parkinson's disease pathogenesis. *Trends Neurosci.* **42**, 4–13 (2019).
62. Albin, R. L., Young, A. B. & Penney, J. B. The functional anatomy of basal ganglia disorders. *Trends Neurosci.* **12**, 366–375 (1989).
63. Ugrumov, M. V. *et al.* Modeling of presymptomatic and symptomatic stages of Parkinsonism in mice. *Neuroscience* **181**, 175–188 (2011).
64. Schapira, A. H. V. Neurobiology and treatment of Parkinson's disease. *Trends Pharmacol. Sci.* **30**, 41–47 (2009).
65. Bové, J. & Perier, C. Neurotoxin-based models of Parkinson's disease. *Neuroscience* **211**, 51–76 (2012).
66. Carnicella, S. *et al.* Implication of dopamine D3 receptor activation in the reversion of Parkinson's disease-related motivational deficits. *Transl. Psychiatry* **4**, e401–e408 (2014).
67. Solari, N., Bonito-Oliva, A., Fisone, G. & Brambilla, R. Understanding cognitive deficits in Parkinson's disease: Lessons from preclinical animal models. *Learn. Mem.* **20**, 592–600 (2013).
68. Faull, R. L. M. & Laverty, R. Changes in dopamine levels in the corpus striatum following lesions in the substantia nigra. *Exp. Neurol.* **23**, 332–340 (1969).
69. Lee, C. S., Sauer, H. & Björklund, A. Dopaminergic neuronal degeneration and motor impairments following axon terminal lesion by intrastriatal 6-hydroxydopamine in the rat. *Neuroscience* **72**, 641–653 (1996).
70. Kirik, D., Rosenblad, C. & Björklund, A. Characterization of behavioral and neurodegenerative changes following partial lesions of the nigrostriatal dopamine system induced by intrastriatal 6-hydroxydopamine in the rat. *Exp. Neurol.* **152**, 259–277 (1998).
71. Bez, F., Francardo, V. & Cenci, M. A. Dramatic differences in susceptibility to l-DOPA-induced dyskinesia between mice that are aged before or after a nigrostriatal dopamine lesion. *Neurobiol. Dis.* **94**, 213–225 (2016).
72. Francardo, V. & Cenci, M. A. Investigating the molecular mechanisms of L-DOPA-induced dyskinesia in the mouse. *Parkinsonism Relat. Disord.* **20**, S20–S22 (2014).

73. Lundblad, M., Picconi, B., Lindgren, H. & Cenci, M. A. A model of L-DOPA-induced dyskinesia in 6-hydroxydopamine lesioned mice: Relation to motor and cellular parameters of nigrostriatal function. *Neurobiol. Dis.* **16**, 110–123 (2004).
74. Bido, S. *et al.* Differential involvement of Ras-GRF1 and Ras-GRF2 in L-DOPA-induced dyskinesia. *Ann. Clin. Transl. Neurol.* **2**, 662–678 (2015).
75. Iancu, R., Mohapel, P., Brundin, P. & Paul, G. Behavioral characterization of a unilateral 6-OHDA-lesion model of Parkinson's disease in mice. *Behav. Brain Res.* **162**, 1–10 (2005).
76. Carvalho, M. M. *et al.* Behavioral characterization of the 6-hydroxidopamine model of Parkinson' s disease and pharmacological rescuing of non-motor deficits. *Mol. Neurodegener.* **8**, 1–11 (2013).
77. Mendes-Pinheiro, B. *et al.* Unilateral intrastriatal 6-hydroxydopamine lesion in mice: A closer look into non-motor phenotype and glial response. *Int. J. Mol. Sci.* **22**, 11530 (2021).
78. Su, R. J. *et al.* Time-course behavioral features are correlated with Parkinson's disease-associated pathology in a 6-hydroxydopamine hemiparkinsonian rat model. *Mol. Med. Rep.* **17**, 3356–3363 (2018).
79. Stephen Fink, J. & Smith, G. P. Mesolimbicocortical dopamine terminal fields are necessary for normal locomotor and investigatory exploration in rats. *Brain Res.* **199**, 359–384 (1980).
80. Arber, S. & Costa, R. M. Networking brainstem and basal ganglia circuits for movement. *Nat. Rev. Neurosci.* **23**, 342–360 (2022).
81. Guatteo, E., Berretta, N., Monda, V., Ledonne, A. & Mercuri, N. B. Pathophysiological features of nigral dopaminergic neurons in animal models of Parkinson's disease. *Int. J. Mol. Sci.* **23**, 4508 (2022).
82. Surmeier, D. J. Determinants of dopaminergic neuron loss in Parkinson's disease. *FEBS J.* **285**, 3657–3668 (2018).
83. Seidl, S. E. & Potashkin, J. A. The promise of neuroprotective agents in Parkinson's disease. *Front. Neurol.* **2**, 1–19 (2011).
84. Erekat, N. S. *Apoptosis and its Role in Parkinson's Disease* (Exon Publications, 2018).
85. Van Nuenen, B. F. L. *et al.* Mapping preclinical compensation in Parkinson's disease: An imaging genomics approach. *Mov. Disord.* **24**, 703–710 (2009).
86. Bezard, E., Gross, C. E. & Brotchie, J. M. Presymptomatic compensation in Parkinson's disease is not dopamine-mediated. *Trends Neurosci.* **26**, 215–221 (2003).
87. Cramb, K. M. L., Beccano-kelly, D., Wade-martins, R. & Cragg, S. J. Impaired dopamine release in Parkinson' s disease. *Brain* **1**, 1–16 (2023).
88. Stoessl, A. J. Positron emission tomography in premotor Parkinson' s disease. *Parkinsonism Relat. Disord.* **13**, 421–424 (2007).
89. Hilker, R. *et al.* Positron emission tomographic analysis of the nigrostriatal dopaminergic system in familial parkinsonism associated with mutations in the Parkin gene. *Ann. Neurol.* **49**, 367–376 (2001).
90. Sun, F. *et al.* Next-generation GRAB sensors for monitoring dopaminergic activity in vivo. *Nat. Methods* **17**, 1156–1166 (2020).
91. Roberts, B. M. *et al.* GABA uptake transporters support dopamine release in dorsal striatum with maladaptive downregulation in a parkinsonism model. *Nat. Commun.* **11**, 1–17 (2020).
92. Sheng, Z. & Cai, Q. Mitochondrial transport in neurons. *Nat. Rev. Neurosci.* **13**, 77–93 (2012).
93. Keating, D. J. Mitochondrial dysfunction, oxidative stress, regulation of exocytosis and their relevance to neurodegenerative diseases. *J. Neurochem.* **104**, 298–305 (2008).
94. German, C. L., Baladi, M. G., McFadden, L. M., Hanson, G. R. & Fleckenstein, A. E. Regulation of the dopamine and vesicular monoamine transporters: Pharmacological targets and implications for disease. *Pharmacol. Rev.* **67**, 1005–1024 (2015).
95. Gomez-lazaro, M. *et al.* 6-Hydroxydopamine activates the mitochondrial apoptosis pathway through p38 MAPK-mediated, p53-independent activation of Bax and PUMA. *J. Neurochem.* **104**, 1599–1612 (2008).
96. Cheng, H., Ulane, C. M. & Burke, R. E. Clinical progression in Parkinson disease and the neurobiology of axons. *Ann. Neurol.* **67**, 715–725 (2010).
97. Tagliaferro, P. & Burke, R. E. Retrograde axonal degeneration in Parkinson disease. *J. Parkinsons. Dis.* **6**, 1–15 (2016).
98. Ureshino, R. P. *et al.* Effects of aging in the striatum and substantia nigra of a Parkinson' s disease animal model. *Toxicol. Pathol.* **46**, 348–358 (2018).
99. Boix, J., von Hieber, D. & Connor, B. Gait analysis for early detection of motor symptoms in the 6-ohda rat model of Parkinson's disease. *Front. Behav. Neurosci.* **12**, 1–15 (2018).
100. Parker, J. G. *et al.* Diametric neural ensemble dynamics in parkinsonian and dyskinetic states. *Nature* **557**, 177–182 (2018).
101. Moghaddam, H. S., Zare-Shahabadi, A., Rahmani, F. & Rezaei, N. Neurotransmission systems in Parkinson's disease. *Rev. Neurosci.* **28**, 509–536 (2017).
102. Giguère, N., Nanni, S. B. & Trudeau, L. E. On cell loss and selective vulnerability of neuronal populations in Parkinson's disease. *Front. Neurol.* **9**, 1–22 (2018).

Acknowledgements

We thank the FENS-Kavli Network of Excellence for fruitful discussions and Dr. László Acsády for helpful comments on the manuscript. This work was supported by the 'Lendület' Program of the Hungarian Academy of Sciences (LP2015-2/2015), NKFIH KH125294, NKFIH K135561, the European Research Council Starting Grant no. 715043 and SPIRITS 2020 of Kyoto University to BH, and by the ÚNKP-20-3 New National Excellence Program of the Ministry for Innovation and Technology to PH. We acknowledge the help of the Nikon Center of Excellence at the Institute of Experimental Medicine (IEM), Nikon Europe, Nikon Austria and Auro-Science Consulting for kindly providing microscopy support. We thank Dr. László Acsády for providing the Nikon Eclipse confocal microscope.

Author contributions

A.S., B.H. and A.W. conceived the study. A.S., P.H., E.R., K.L., N.S., A.K., D.B., B.B., E.A., F.M. performed the research. A.S., P.H. and B.H. wrote the manuscript. All authors reviewed the manuscript.

Competing interests

The authors declare no competing interests.

Additional information

Supplementary Information The online version contains supplementary material available at https://doi.org/10.1038/s41598-023-46576-0.

Correspondence and requests for materials should be addressed to A.S., A.W. or B.H.